

---

**ZINC OXIDE:  
NEW INSIGHTS INTO A  
MATERIAL FOR ALL AGES**

---

**BY**

**AMIR MOEZZI**

**BSc. Chemical Engineering**

**A Dissertation Submitted for the  
Degree of Doctor of Philosophy**

**University of Technology Sydney**

**2012**

## **Certificate of authorship/originality**

I certify that the work in this thesis has not previously been submitted for a degree nor has it been submitted as part of requirements for a degree except as fully acknowledged within the text.

I also certify that the thesis has been written by me. Any help that I have received in my research work and the preparation of the thesis itself has been acknowledged. In addition, I certify that all information sources and literature used are indicated in the thesis.

Production Note:  
Signature removed prior to publication.

Amir Moezzi

11/10/2012

Copyright © 2012 by Amir Moezzi

All rights reserved. No part of this publication may be reproduced, distributed, or transmitted in any form or by any means, including photocopying, recording, or other electronic or mechanical methods, without the prior written permission of the author, except in the case of brief quotations embodied in critical reviews and certain other non-commercial uses permitted by copyright law.

Printed and bound in Australia

## Acknowledgements

I would like to express my special appreciation to the company PT. Indo Lysaght, of Indonesia, for financial support for my project and very kind hospitality during the visits from their chemical plants.

My greatest debts are to my principal supervisor, Prof. Michael Cortie, and my co-supervisors Dr Andrew McDonagh, who gave me the opportunity to undertake this project and for their support and encouragement throughout the project. I learned so much working with you and I am really grateful for your time and effort teaching me how to do high quality research and produce interesting and important results. I also thank you for editorial help in my thesis.

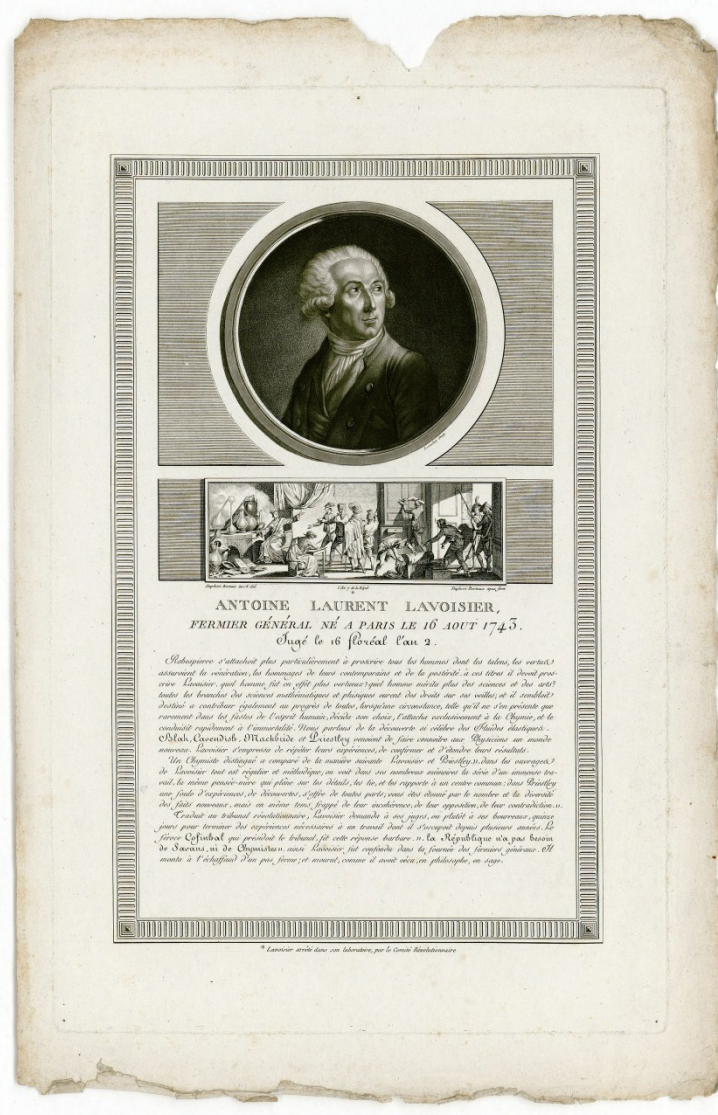
Thanks to my family for their encouragement despite a long distance between us.

Very special thank to Dr Ronald Shimmon for his extensive care and support. Also I would like to express my appreciation to Drs R. Wuhler, M. Berkahn, A. Dowd, M. Philips, C. Ton-That, P. Thomas and L. Xiao. I also thank Mr J-P. Guerbois for his help in performing TGA and MS, Mrs S. Fenech and Mrs G. Armstrong for their help in using nitrogen measurement instrument and also Mr D. Bishop for performing the ICP-MS test. Thanks to Miss V. Schrameyer for her help in translation of German papers into English.

Sincere thanks to my fellow friends specially Mr M. Coutts for their patience and listening to long and sometimes boring discussions that we had during this period.

Thanks to Drs P. Robinson (Canada), S. Mahmud (Malaysia) and P. Stamford (Australia) for their helpful responses to our questions. Thanks to Dr H. Nguyen, from School of Chemical Engineering at UNSW for some of the BET surface area measurements and Dr K. Kannangara from School of Science and Health, UWS for solid-NMR. Support from companies for providing photographs for my publication is highly appreciated. Thanks to the Microstructural Analysis Unit (MAU) at UTS for providing me with the state-of-the-art equipment and facilities to analyse the materials. Thanks to Australian Synchrotron in Melbourne for the time they provided for the synchrotron radiation studies in this work.

Last but not least, I thank all of my friends who supported me with patience in my project.



Antoine Laurent Lavoisier (1743-1794), “father of modern chemistry”, in 1789 for the first time suggested that “Flowers of zinc” be named “zinc oxide” reflecting the elements in the nomenclature of compound.

*"We think only through the medium of words. Languages are true analytical methods. Algebra, which is adapted to its purpose in every species of expression, in the most simple, most exact, and best manner possible, is at the same time a language and an analytical method. The art of reasoning is nothing more than a language well arranged."*

Antoine Laurent Lavoisier, *Traité Élémentaire de Chimie*, 1789

Adopted from translation by Robert Kerr, 1790

## Table of Contents

	<b>Page</b>
<b>Certificate of authorship/originality</b>	<b>ii</b>
<b>Acknowledgements</b>	<b>iii</b>
<b>Table of Contents</b>	<b>v</b>
<b>List of Figures</b>	<b>x</b>
<b>List of Tables</b>	<b>xviii</b>
<b>List of Schemes</b>	<b>xix</b>
<b>Abbreviations</b>	<b>xx</b>
<b>Publications and conference presentations associated with this work</b>	<b>xxiv</b>
<b>Abstract</b>	<b>xxv</b>
<b>Chapter 1: Zinc Oxide: Synthesis, Properties and Applications</b>	<b>2</b>
1.1. INTRODUCTION AND OVERVIEW OF THE DISSERTATION	2
1.2. HISTORICAL ASPECTS	5
1.3. SYNTHESIS	8
1.3.1. <i>Background</i>	8
1.3.2. <i>Industrial production methods</i>	10
Pyrometallurgical synthesis	11
Hydrometallurgical synthesis	29
ZnO as a by-product from other processes	30
Production of “active” zinc oxide by decomposition of hydrozincite	31
1.3.3. <i>Small-scale production routes</i>	35
Precipitation of Zn(OH) <sub>2</sub> or ZnO from aqueous solutions of zinc salts	35
Solvent extraction and pyrolysis of zinc nitrate	35
Deposition of thin films	36
Gas-phase synthesis	36
Miscellaneous other methods	37
1.4. PROPERTIES	38
1.4.1. <i>Crystal structures</i>	39
1.4.2. <i>Toxicology</i>	40
1.4.3. <i>Morphology of zinc oxide particles</i>	41
1.4.4. <i>Industrial grades</i>	42
Bulk zinc oxide	42
Active zinc oxide by calcination of a carbonate	43
Other ‘wet-process’ ZnO	43
	v

---

ZnO single crystals	44
1.4.5. <i>Optical properties</i>	44
1.4.6. <i>Electrical, thermal and magnetic properties</i>	45
Piezoelectricity, pyroelectricity and thermoelectricity	45
Ferroelectricity, magnetism and ferromagnetism	46
Electrical conductivity	46
Heat capacity, thermal conductivity, thermal expansion coefficient	48
Thermochromism	48
1.4.7. <i>Surface properties</i>	48
1.5. APPLICATIONS	49
1.5.1. <i>Rubber</i>	49
1.5.2. <i>Ceramics and concrete</i>	54
1.5.3. <i>Plastics and linoleum</i>	55
1.5.4. <i>Pigments and coatings</i>	56
1.5.5. <i>Cosmetics, medical and dental</i>	57
1.5.6. <i>Catalysts</i>	59
1.5.7. <i>Desulfurisation</i>	61
1.5.8. <i>Oil and gas well drilling fluid</i>	63
1.5.9. <i>Varistors</i>	63
1.5.10. <i>Fertilisers, food supplements and animal feed</i>	65
1.5.11. <i>Zinc oxide in chemical synthesis</i>	67
1.5.12. <i>Miscellaneous applications</i>	70
1.6. POTENTIAL AND EMERGING APPLICATIONS	71
1.6.1. <i>Liquid crystal displays (LCDs)</i>	71
1.6.2. <i>Light emitting diodes (LEDs)</i>	72
1.6.3. <i>Spintronics</i>	72
1.6.4. <i>Solar cells</i>	72
1.6.5. <i>Sensors and actuators</i>	73
1.6.6. <i>ZnO in textiles</i>	73
1.7. CONCLUSIONS	73
<b>Chapter 2: Single-Stage Process to Synthesise Zinc Oxide Using Sodium Hydroxide</b>	<b>76</b>
2.1. INTRODUCTION	76
2.2. EXPERIMENTAL	80
2.2.1. <i>General</i>	80
2.2.2. <i>Reactant stoichiometry</i>	81
2.2.3. <i>Method of combining the reactants</i>	81
2.2.4. <i>Reaction temperature</i>	82
2.3. RESULTS AND DISCUSSION	82
2.3.1. <i>The effect of reactant stoichiometry</i>	82

---

2.3.2. <i>Method of combining reactants</i>	87
2.3.3. <i>The effect of temperature</i>	90
2.3.4. <i>Fluorescence spectroscopy</i>	93
2.3.5. <i>The catalytic effect of OH</i>	95
2.4. CONCLUSIONS	98
<b>Chapter 3: A Single-Stage Process to Synthesise Zinc Oxide Using Ammonia</b>	<b>100</b>
3.1. INTRODUCTION	100
3.2. EXPERIMENTAL	101
3.3. RESULTS AND DISCUSSION	102
3.3.1. <i>Characterisation and thermogravimetric analysis</i>	102
3.3.2. <i>Microscopy and BET surface area measurement</i>	103
3.3.3. <i>Fluorescence spectroscopy</i>	105
3.3.4. <i>The catalytic role of NH<sub>3</sub> and OH</i>	105
3.4. CONCLUSIONS	108
<b>Chapter 4: Multi-Stage Routes to Synthesise Zinc Oxide Using Zinc Peroxide</b>	<b>110</b>
4.1. INTRODUCTION	110
4.2. EXPERIMENTAL	111
4.2.1. <i>General</i>	111
4.2.2. <i>Synthesis</i>	111
ZnO <sub>2</sub> via zinc acetate and H <sub>2</sub> O <sub>2</sub> reaction	111
ZnO from as-synthesised ZnO <sub>2</sub>	111
ZnO <sub>2</sub> via Zn <sub>4</sub> SO <sub>4</sub> (OH) <sub>6</sub> ·4H <sub>2</sub> O and H <sub>2</sub> O <sub>2</sub> reaction	112
ZnO from as-synthesised ZnO <sub>2</sub>	112
4.3. RESULTS AND DISCUSSION	112
4.3.1. <i>Characterisation</i>	112
Products from reaction of zinc acetate and H <sub>2</sub> O <sub>2</sub>	112
Products from reaction of Zn <sub>4</sub> SO <sub>4</sub> (OH) <sub>6</sub> ·4H <sub>2</sub> O and H <sub>2</sub> O <sub>2</sub>	113
4.3.2. <i>Thermogravimetric analysis</i>	114
4.3.3. <i>Mechanisms of formation of zinc peroxide</i>	115
Zinc acetate-H <sub>2</sub> O <sub>2</sub> route	115
Zn <sub>4</sub> SO <sub>4</sub> (OH) <sub>6</sub> ·4H <sub>2</sub> O-H <sub>2</sub> O <sub>2</sub> route	116
4.4. CONCLUSIONS	118
<b>Chapter 5: Multi-Stage Routes to Synthesise Zinc Oxide Using Zinc Hydroxy Salts</b>	<b>120</b>
5.1. INTRODUCTION	120
5.2. EXPERIMENTAL	121
5.2.1. <i>General</i>	121
5.2.2. <i>Synthesis of zinc hydroxy salts</i>	123
Zinc hydroxy carbonate	123

---

Zinc hydroxy sulphate	123
Zinc hydroxy chloride	123
Zinc hydroxy nitrate	124
Zinc hydroxy acetate	124
Product of reaction between zinc hydroxy acetate and ethanol	124
5.2.3. <i>Synthesis of ZnO from zinc hydroxy salts</i>	125
5.3. RESULTS AND DISCUSSION	125
5.3.1. <i>Zinc hydroxy carbonate</i>	125
Characterisation, TGA-DTA and microscopy	126
Real-time synchrotron radiation study	129
BET surface area measurements	130
5.3.2. <i>Zinc hydroxy sulphate</i>	132
Characterisation and TGA-DTA	132
Synchrotron radiation study and TGA-MS	134
Microscopy and BET surface area measurement	141
Mechanism	142
5.3.3. <i>Zinc hydroxy chloride</i>	143
Characterisation, BET surface area measurement and microscopy	146
Synchrotron radiation study, TGA-DTA and TGA-MS	148
TGA-MS	152
Sublimation test	153
Mechanism	156
5.3.4. <i>Zinc hydroxy nitrate</i>	157
Characterisation, BET surface area measurement and microscopy	157
Synchrotron radiation study and TGA-DTA	159
TGA-MS	161
Mechanism	169
5.3.5. <i>Zinc hydroxy acetate</i>	170
Characterisation, BET surface area measurement and microscopy	176
FTIR spectroscopy	178
CP-MAS <sup>13</sup> C NMR	180
TGA-DTA	181
Synchrotron radiation study	182
TGA-MS	186
Evidence for the formation of sublimate	191
Mechanism	193
Reactivity of zinc hydroxy acetate dihydrate with ethanol	193
5.3.6. <i>Comparison</i>	200
TGA	200
XRD	201



---

Fluorescence spectroscopy	202
BET specific surface area	205
5.4. CONCLUSIONS	205
<b>Chapter 6: Mechanistic and Kinetic Aspects of the Solid/liquid Pathway for the Formation of Zinc Hydroxy Nitrate</b>	<b>208</b>
6.1. INTRODUCTION	208
6.2. EXPERIMENTAL	210
6.2.1. <i>General</i>	210
6.2.2. <i>Synthesis</i>	210
6.2.3. <i>Kinetics</i>	211
6.2.4. <i>Determination of solubility of zinc hydroxy nitrate</i>	211
6.3. RESULTS AND DISCUSSION	212
6.3.1. <i>Characterisation and stoichiometry of the reaction</i>	212
6.3.2. <i>Thermodynamics</i>	217
6.3.3. <i>Kinetics</i>	222
6.3.4. <i>Solubility</i>	229
6.3.5. <i>Mechanism and catalytic role of H<sup>+</sup></i>	230
6.4. CONCLUSIONS	231
<b>Chapter 7: General Conclusions and Future Directions</b>	<b>234</b>
7.1. GENERAL CONCLUSIONS	234
7.2. FUTURE DIRECTIONS	236
<b>Appendix</b>	<b>239</b>
<b>References</b>	<b>245</b>

## List of Figures

	Page
<b>Figure 1.1.</b> Number of scientific publications on zinc oxide since 1882 until 2011. Data available from literature database Scopus (keyword: “zinc oxide”).....	2
<b>Figure 1.2.</b> Advertisement label for zinc oxide, 1868. (USA Library of Congress. <a href="http://www.loc.gov/pictures/item/2006679062/">http://www.loc.gov/pictures/item/2006679062/</a> Reproduction Number: LC-USZ62-51233).....	8
<b>Figure 1.3.</b> Chart showing the various uses of zinc metal. Zinc oxide is the main chemical produced from zinc metal. Compiled using data from diverse sources. ....	9
<b>Figure 1.4.</b> Schematic of the indirect process to produce ZnO reproduced from the 1850 US patent of Leclair and Barruel [45]. ....	12
<b>Figure 1.5.</b> Photograph of a French process drum in operation, by permission from PT. Indo Lysaght, Indonesia. ....	13
<b>Figure 1.6.</b> A typical bag-house design reproduced from the US patent 6786946. ....	14
<b>Figure 1.7.</b> The Metallurgical Zinc Recovery (MZR) system for the separation of metallic zinc from zinc ash. From Pyrotek technical documents [51, 52]. ....	15
<b>Figure 1.8.</b> SEM images of the French process ZnO (samples from PT. Indo Lysaght, Indonesia; images by Dr R. Wuhler, University of Technology Sydney). ....	16
<b>Figure 1.9.</b> Process flow diagram (PFD) of the French process. ....	17
<b>Figure 1.10.</b> Schematic of the Larvik process designed by Lundevall [55].....	18
<b>Figure 1.11.</b> Graph of melting and boiling points of the first transition series elements, Cd and Pb. ....	19
<b>Figure 1.12.</b> Zinc oxide rotary kiln. Picture by Henan Bailing Machinery Co. [58]. ....	20
<b>Figure 1.13.</b> Ellingham diagram showing free energy change of indicated reactions as a function of temperature, calculated using standard state thermodynamic data for the species. ....	21
<b>Figure 1.14.</b> Effect of temperature and gas composition on the partial pressure of Zn <sub>(g)</sub> (in atm). A decrease in temperature or CO/CO <sub>2</sub> causes a reduction in p <sub>Zn</sub> due to increased oxidation. Recalculated and redrawn after Schoukens <i>et al.</i> , [61]. Atmospheric pressure is assumed.....	22
<b>Figure 1.15.</b> Typical process flow diagram of the Waelz process with permission from ValoRes GmbH [66]. Note: in the American process the ‘process air pipe’ shown in the PFD above is not normally used (private communication with Dr Juergen Ruetten, ValoRes GmbH). ....	24
<b>Figure 1.16.</b> Waelz kiln Sections [66]. ....	25
<b>Figure 1.17.</b> Specific surface area of ZnO vs. pyrolysis temperature using zinc acetate dihydrate 32.6% (w/v) aqueous solution [49].....	26
<b>Figure 1.18.</b> Process flow diagram (PFD) of spray pyrolysis of aqueous solution of zinc salts to ZnO. ..	26
<b>Figure 1.19.</b> Schematics of (left) submerged plasma process [77] and (right) Mintek’s Enviroplas process for zinc fuming [72]. ....	28
<b>Figure 1.20.</b> (a) Zinc ash; (b) zinc dross. © Commonwealth of Australia 2001 [78]. Photographs courtesy of Environment Australia. ....	29
<b>Figure 1.21.</b> Schematic of the sodium dithionite process [83]. ....	30

<b>Figure 1.22.</b> Free energy change for reaction $Zn_5(CO_3)_2(OH)_6 \rightleftharpoons 5ZnO + 2CO_2 + 3H_2O$ , calculated by the authors using published thermochemical data [88, 89].	31
<b>Figure 1.23.</b> Fully hydroxylated ZnO crystal [8].	33
<b>Figure 1.24.</b> Schematic of the rotary kiln for the calcination of basic zinc carbonate as depicted in US patent 2603554 [95].	34
<b>Figure 1.25.</b> Organic solvent extraction process for the production of zinc oxide [62].	36
<b>Figure 1.26.</b> Arc discharge method schematic, reproduced from [107].	37
<b>Figure 1.27.</b> Unit cell of the crystal structure of ZnO. (a) Hexagonal wurtzite structure, (b) “zinc-blende” structure and (c) cubic rock-salt structure [2].	39
<b>Figure 1.28.</b> SEM images of ZnO showing various morphologies; (a) and (b) are reprinted with permission from [110], (c) from [111], (d) from [99], (e) from [140], (g) from [132], (h) from [98] and (f) is synthesised by the authors. Reproduced with permission from the various sources cited.	42
<b>Figure 1.29.</b> Zinc oxide single crystal, produced by the hydrothermal method. Image courtesy of Tokyo Denpa Co., Ltd. Japan.	44
<b>Figure 1.30.</b> Mechanism for reaction of zinc oxide and the vulcanisation accelerator [193].	51
<b>Figure 1.31.</b> Schematic and photograph of Banbury mixer in tire manufacturing. Reproduced from technical document from Farrel corporation.	52
<b>Figure 1.32.</b> Fate of zinc oxide in tire.	53
<b>Figure 1.33.</b> Examples of methanol synthesis converters: (a) tube-cooled, low-pressure reactor; (b) quench-cooled, low-pressure reactor [224]. Adopted from Catalyst Handbook, ed. M.V. Twigg, Manson Publishing Company, London, 1996).	60
<b>Figure 1.34.</b> a. An industrial desulfurisation unit; b. A schematic diagram of a simplified hydrocarbon feedstock purification unit using ZnO as a desulfurisation absorbent; c. An example of a ZnO desulfurisation absorbent. By permission from Haldor Topsøe, Denmark.	62
<b>Figure 1.35.</b> (a) Schematic of microstructure of a ZnO varistor [10]; (b) small size varistor; (c) temperature dependence of I-V curve of ZnO varistor [232] and (d) a typical silicone-rubber-housed ZnO surge arrester type PEXLIM P330-YH420 suitable for protection in 420 kV systems by permission from ABB, Sweden.	64
<b>Figure 1.36.</b> PFD of production of zinc phosphate from zinc oxide.	68
<b>Figure 1.37.</b> PFD of production of zinc borate from zinc oxide.	69
<b>Figure 2.1.</b> Thermodynamic parameters for the reaction of solid $\epsilon$ -Zn(OH) <sub>2</sub> to solid ZnO and H <sub>2</sub> O. The values are computed from the standard states at 298 °K at 1 atmosphere using the specific heat capacities from reference [287].	79
<b>Figure 2.2.</b> X-ray diffraction data obtained from the products of reactions A, B and C. The diffraction pattern for product C corresponds to pure ZnO (wurtzite). The peaks assigned to ZnO are indicated by * in the data for A and B. Other peaks in A and B correspond to $\epsilon$ -Zn(OH) <sub>2</sub> .	83
<b>Figure 2.3.</b> XRD on the products of reactions (D) to (H) shows patterns, which conform with zinc oxide.	83
<b>Figure 2.4.</b> Thermogravimetric analysis data for the products of Reactions A, B and C. Heating rate was 5 °C min <sup>-1</sup> in an N <sub>2</sub> atmosphere.	84

<b>Figure 2.5.</b> TGA comparison charts on the products of reactions (C) to (H) shows no decomposition at 120 °C. Mass loss up to the temperature of 120 °C is attributed to moisture removal and the mass loss over 120 °C is attributed to surface hydroxyl groups removal.....	84
<b>Figure 2.6.</b> SEM images of the products of reactions A (left) and B (right). From reaction (A) smaller ellipsoidal particles are formed on top of the big plate-like structures. In (B), plate-like structures cannot be detected and smaller star-like particles are dominant.....	85
<b>Figure 2.7.</b> SEM images of ZnO particles produced by the reactions C to H.....	86
<b>Figure 2.8.</b> XRD associated with zinc hydroxide sulphate tetrahydrate, $Zn_4SO_4(OH)_6 \cdot 4H_2O$ (JCPDF card 00-044-0673).....	87
<b>Figure 2.9.</b> TGA on the as-produced $Zn_4SO_4(OH)_6 \cdot 4H_2O$ .....	87
<b>Figure 2.10.</b> XRD data of the reaction products prepared at 70 °C using different feeding methods: (a) NaOH solution added to $ZnSO_4$ solution in a single addition; (b) NaOH solution added to $ZnSO_4$ solution in a dropwise manner; (c) $ZnSO_4$ solution added to NaOH solution in a single shot; (d) $ZnSO_4$ solution added to NaOH solution in a dropwise manner.....	88
<b>Figure 2.11.</b> SEM images of ZnO particles produced at 70 °C with different feeding methods. (a) NaOH solution added to $ZnSO_4$ solution in a single addition; (b) NaOH solution added to $ZnSO_4$ solution in a drop-wise manner; (c) $ZnSO_4$ solution added to NaOH solution in a single addition; (d) $ZnSO_4$ solution added to NaOH solution in a drop-wise manner.....	89
<b>Figure 2.12.</b> XRD shows ZnO hexagonal wurtzite structure for all the samples made at different temperatures from 25 °C to 90 °C.....	91
<b>Figure 2.13.</b> SEM images of ZnO particles synthesised at different temperatures.....	92
<b>Figure 2.14.</b> BET specific surface area ( $m^2/g$ ) vs. reaction temperature in the range of 25 to 90 °C. The trend line shown was obtained by polynomial regression and is provided as a guide to the eye.....	93
<b>Figure 2.15.</b> RT fluorescence emission spectra of ZnO powder samples: French process ZnO; (I) ZnO product where the zinc sulphate solution was added to the sodium hydroxide solution in a drop-wise manner over 3 minutes according to Section 2.3.2; (II) and (III) ZnO products from reactions at 80 °C and 60 °C according to Section 2.3.3, respectively. Excitation wavelength = 310 nm, excitation slit width = 5 nm (little steps at 460 and 570 nm are artefacts due to filter changes).....	94
<b>Figure 3.1.</b> X-ray diffraction data obtained from the product of reaction between zinc sulphate and ammonia correspond to pure ZnO (wurtzite), JCPDF card 01-089-7102.....	103
<b>Figure 3.2.</b> TGA on the ZnO product. Mass loss up to the temperature of 120 °C is attributed to moisture removal and the mass loss over 120 °C is attributed to removal of surface hydroxyl groups.....	103
<b>Figure 3.3.</b> SEM images of zinc oxide crystals produced at 65 °C by feeding the zinc sulphate in a drop-wise manner to the ammonia solution.....	104
<b>Figure 3.4.</b> RT fluorescence emission spectra of ZnO powder sample made by drop-wise addition of zinc sulphate solution to ammonia over 3 minutes according to section 3.2. Excitation wavelength = 310 nm, excitation slit width = 5 nm (little steps at 460 and 570 nm are artefacts due to filter changes).....	105
<b>Figure 4.1.</b> XRD on (bottom) product of the reaction between zinc acetate and hydrogen peroxide corresponds to zinc peroxide (JCPDF card 01-077-2414) and (top) product of calcination of as-produced	

zinc peroxide corresponds to zinc oxide (JCPDF card 01-075-0576). Peaks marked with “*” are associated with zinc peroxide.....	113
<b>Figure 4.2.</b> XRD on (bottom) product of the reaction between $Zn_4SO_4(OH)_6 \cdot 4H_2O$ and $H_2O_2$ corresponds to $ZnO_2$ (JC-PDF 01-077-2414) and (top) product of calcination of as-produced $ZnO_2$ corresponds to mainly to ZnO (JC-PDF 00-001-1136) and some remaining $ZnO_2$ . Peaks marked with “*” are associated with zinc peroxide. ....	113
<b>Figure 4.3.</b> TGA on zinc peroxide made from (I) zinc acetate- $H_2O_2$ route and (II) $Zn_4SO_4(OH)_6 \cdot 4H_2O$ - $H_2O_2$ route. ....	114
<b>Figure 4.4.</b> DTA on zinc peroxide made from (I) zinc acetate- $H_2O_2$ route and (II) $Zn_4SO_4(OH)_6 \cdot 4H_2O$ - $H_2O_2$ route. ....	115
<b>Figure 4.5.</b> SEM image on nano-particles of $ZnO_2$ made via zinc acetate- $H_2O_2$ route. ....	116
<b>Figure 4.6.</b> SEM image on ZnO particles made via zinc acetate- $H_2O_2$ route. ....	116
<b>Figure 4.7.</b> SEM image on $ZnO_2$ made via $Zn_4SO_4(OH)_6 \cdot 4H_2O/H_2O_2$ route. ....	117
<b>Figure 4.8.</b> SEM images on ZnO/ $ZnO_2$ particles made via $Zn_4SO_4(OH)_6 \cdot 4H_2O-H_2O_2$ route. ....	117
<b>Figure 5.1.</b> XRD (Cu $K\alpha$ ) on the product corresponding to hydrozincite (JC-PDF card 00-019-1458). The peaks are broad.....	126
<b>Figure 5.2.</b> TGA-DTA on hydrozincite.....	127
<b>Figure 5.3.</b> XRD (Cu $K\alpha$ ) on the calcined product corresponds to ZnO (JC-PDF card 00-005-0664). ..	127
<b>Figure 5.4.</b> SEM images of (A) BZC; (B) highly porous ZnO produced from calcination of BZC. ....	128
<b>Figure 5.5.</b> TEM images on the ZnO particles produced from calcination of BZC (courtesy of Dr A. Dowd).....	128
<b>Figure 5.6.</b> Colour-coded contour XRD (synchrotron) graph shows the real-time transformation of hydrozincite to ZnO. The intensity is colour-coded. ....	129
<b>Figure 5.7.</b> Two projections of 3D-stacked XRD (synchrotron) patterns on BZC show that intensity of BZC is lower than that of the end-product ZnO. ZnO peaks are intensified by increasing the temperature. ....	130
<b>Figure 5.8.</b> XRD (Cu $K\alpha$ ) on the products of calcination of BZC at a temperature range of 250-350 °C for 1 hour shows only ZnO peaks. ....	131
<b>Figure 5.9.</b> BET specific surface area of ZnO samples prepared by calcination of BZC at 250-350 °C. ....	131
<b>Figure 5.10.</b> XRD (Cu $K\alpha$ ) on the BZS tetrahydrate and the phase, which is believed to be BZS monohydrate.....	133
<b>Figure 5.11.</b> TGA on BZS tetrahydrate and monohydrate. ....	133
<b>Figure 5.12.</b> DTA on BZS tetrahydrate and monohydrate. ....	134
<b>Figure 5.13.</b> Colour-coded contour XRD (synchrotron) graph shows the real-time transformation of $BZS \cdot 4H_2O$ to ZnO. The intensity is colour-coded. ....	134
<b>Figure 5.14.</b> Two projections of 3D-stacked XRD (synchrotron) graphs on $BZS \cdot 4H_2O$ . ....	135
<b>Figure 5.15.</b> Top pattern: XRD pattern on the calcined $BZS \cdot 4H_2O$ at 113 °C obtained by synchrotron radiation (synchrotron $2\theta$ values are converted to the equivalent of Cu $K\alpha$ ). Bottom pattern: XRD (Cu $K\alpha$ ) pattern on unidentified BZS. The two patterns match perfectly with each other. ....	136

<b>Figure 5.16.</b> Stacked XRD (synchrotron) on the BZS·4H <sub>2</sub> O under calcination shows a dynamic phase transformation due to the dehydration by increasing the temperature.....	137
<b>Figure 5.17.</b> XRD pattern on the calcine at 204 °C obtained by synchrotron radiation (synchrotron 2θ value is converted to its equivalent of Cu Kα). .....	137
<b>Figure 5.18.</b> XRD pattern on the calcined sample at 555 °C obtained by synchrotron radiation (synchrotron 2θ value is converted to its equivalent of Cu Kα). ZnO peaks (JC-PDF 01-089-7102) are indicated by “*”. The remaining peaks have been identified as Zn <sub>5</sub> O <sub>2</sub> (SO <sub>4</sub> ) <sub>3</sub> (JC-PDF 00-016-0305)....	139
<b>Figure 5.19.</b> TGA-MS graphs on aged BZS·H <sub>2</sub> O. Shown ion intensities for H <sub>2</sub> O, O <sub>2</sub> , CO <sub>2</sub> , SO <sub>2</sub> and SO <sub>3</sub> are ×10 <sup>9</sup> , ×10 <sup>10</sup> , ×10 <sup>11</sup> , ×10 <sup>10</sup> and ×10 <sup>13</sup> , respectively. ....	140
<b>Figure 5.20.</b> XRD on the product of calcination of BZS at 900 °C shows ZnO peaks.....	141
<b>Figure 5.21.</b> SEM images on (A) precursor and (B) ZnO particles made from that.....	141
<b>Figure 5.22.</b> XRD results on (a) BZCl; (b) calcined BZCl for 2 hours at 400 °C; (c) calcined BZCl for 6 hours at 400 °C and (d) calcined BZCl for 6 hours at 400 °C plus 4 hours at 600 °C. Peaks marked with ♠ in (b) and (c) correspond to ZnO·ZnCl <sub>2</sub> ·2H <sub>2</sub> O and the peaks indicated with ♣ correspond to Zn <sub>5</sub> (OH) <sub>8</sub> Cl <sub>2</sub> ·H <sub>2</sub> O.....	147
<b>Figure 5.23.</b> SEM images of (A) BZCl and (B) ZnO made of that. ....	148
<b>Figure 5.24.</b> Colour-coded contour XRD (synchrotron) graph shows the real-time transformation of BZCl to ZnO. The intensity is colour-coded.....	148
<b>Figure 5.25.</b> Two projections of 3D-stacked XRD (synchrotron) graphs on BZCl.....	149
<b>Figure 5.26.</b> TGA-DTA on the freshly made BZCl and aged BZCl after 13 months.....	150
<b>Figure 5.27.</b> TGA-MS graph on aged BZCl under air atmosphere with a heating rate of 3 °C min <sup>-1</sup> . Shown I <sub>18</sub> for H <sub>2</sub> O, I <sub>36</sub> for HCl, I <sub>44</sub> for CO <sub>2</sub> and I <sub>136</sub> for ZnCl <sub>2</sub> are ×10 <sup>9</sup> , ×10 <sup>12</sup> , ×10 <sup>11</sup> and ×10 <sup>14</sup> , respectively. ....	153
<b>Figure 5.28.</b> Sublimation set-up to trap the volatile zinc-containing material.....	154
<b>Figure 5.29.</b> TGA-DTA on ZnCl <sub>2</sub> ·2H <sub>2</sub> O and ZnCl <sub>2</sub> sublimate collected. ....	155
<b>Figure 5.30.</b> XRD conducted at 100-120 °C and time per step = 5.6 s on the zinc-containing sublimate matches with α and β-zinc chlorides. Peaks marked with * are associated with β-ZnCl <sub>2</sub> (JC-PDF 01-072-1284) and the rest are related to α-ZnCl <sub>2</sub> (JC-PDF 01-074-0519) with major peaks located at 2θ = 18.5 ° and 29 °. ....	155
<b>Figure 5.31.</b> XRD results on (bottom graph) BZN; (middle graph) calcined BZN for 1 hour at 250 °C; (top graph) calcined BZN for 1 hour at 250 °C plus 1 hour at 300 °C. ....	158
<b>Figure 5.32.</b> SEM images of (A) BZN and (B) ZnO made of that. ....	158
<b>Figure 5.33.</b> Colour-coded contour XRD (synchrotron) graph shows the real-time transformation of BZN to ZnO. The intensity is colour-coded.....	159
<b>Figure 5.34.</b> Two projections of 3D-stacked XRD (synchrotron) graphs on BZN.....	160
<b>Figure 5.35.</b> TGA-DTA on BZN.....	161
<b>Figure 5.36.</b> TGA-MS graphs for MS1. I <sub>12</sub> for C <sup>+</sup> and I <sub>44</sub> are shown ×10 <sup>12</sup> and ×10 <sup>11</sup> , respectively. I <sub>18</sub> for H <sub>2</sub> O, I <sub>32</sub> for O <sub>2</sub> , I <sub>30</sub> for NO, I <sub>46</sub> for NO <sub>2</sub> and I <sub>63</sub> for HNO <sub>3</sub> are shown ×10 <sup>9</sup> , ×10 <sup>10</sup> , ×10 <sup>10</sup> , ×10 <sup>12</sup> and ×10 <sup>14</sup> , respectively. ....	162

<b>Figure 5.37.</b> TGA-MS graphs for MS2. $I_{18}$ for $\text{H}_2\text{O}$ , $I_{30}$ for NO, $I_{46}$ for $\text{NO}_2$ and $I_{32}$ for $\text{O}_2$ are shown $\times 10^9$ , $\times 10^{10}$ , $\times 10^{11}$ and $\times 10^{12}$ , respectively. ....	162
<b>Figure 5.38.</b> TGA-MS graphs for MS3. $I_{44}$ ( $\times 10^{11}$ ) for $\text{N}_2\text{O}$ or $\text{CO}_2$ is indicated by ♣. $I_{63}$ ( $\times 10^{14}$ ) for $\text{HNO}_3$ by ♠ and $I_{30}$ ( $\times 10^{10}$ ) for NO is indicated ♥ by and $I_{46}$ ( $\times 10^{11}$ ) for $\text{NO}_2$ is indicated by ♦. $I_{18}$ for $\text{H}_2\text{O}$ and $I_{32}$ for $\text{O}_2$ are Shown $\times 10^9$ and $\times 10^{10}$ , respectively. ....	163
<b>Figure 5.39.</b> TGA-MS graphs for MS4. $I_{18}$ for $\text{H}_2\text{O}$ and $I_{30}$ for NO and $I_{46}$ for $\text{NO}_2$ are shown $\times 10^9$ , $\times 10^{10}$ and $\times 10^{10}$ , respectively. ....	163
<b>Figure 5.40.</b> TGA-MS graphs for MS5. $I_{44}$ and $I_{18}$ for $\text{H}_2\text{O}$ and $I_{32}$ for $\text{O}_2$ and $I_{63}$ for $\text{HNO}_3$ are shown $\times 10^{10}$ , $\times 10^9$ and $\times 10^{13}$ , respectively. Shown $I_{30}$ for NO and $I_{46}$ for $\text{NO}_2$ are $\times 10^{10}$ and $\times 10^{11}$ , respectively. ....	164
<b>Figure 5.41.</b> $I_{18}$ ( $\text{H}_2\text{O}^+$ ) curves for various heating rates. ....	165
<b>Figure 5.42.</b> TGA comparative graphs obtained during TGA-MS tests. ....	166
<b>Figure 5.43.</b> Fraction of ionic currents for NO (X), $\text{NO}_2$ (Y) and $\text{O}_2$ (Z) vs. rate of heating. ....	167
<b>Figure 5.44.</b> TGA-MS on $\text{Zn}(\text{NO}_3)_2 \cdot 6\text{H}_2\text{O}$ under argon with a heating rate of $4\text{ }^\circ\text{C min}^{-1}$ . It can be seen that decomposition of $\text{Zn}(\text{NO}_3)_2$ undergoes completion at temperatures over $324\text{ }^\circ\text{C}$ with the release of nitrogen oxide species. $I_{18}$ for $\text{H}_2\text{O}$ , $I_{32}$ for $\text{O}_2$ , $I_{30}$ for NO, $I_{46}$ for $\text{NO}_2$ and $I_{44}$ are shown $\times 10^9$ , $\times 10^9$ and $\times 10^9$ , $\times 10^{10}$ and $\times 10^{10}$ , respectively. ....	168
<b>Figure 5.45.</b> X-ray diffraction pattern of as-synthesised BZA. The positions of $d$ -spacings at 1.42 and 1.49 nm are resolved from synchrotron data using Split-Pearson VII distribution function. ....	176
<b>Figure 5.46.</b> XRD ( $\text{Cu K}\alpha$ ) on the product shows peaks associated with ZnO. ....	177
<b>Figure 5.47.</b> SEM images of (A) BZA and (B) the calcination product, ZnO. ....	177
<b>Figure 5.48.</b> Transmission electron images of the ZnO nanocrystals formed by calcination at $400\text{ }^\circ\text{C}$ . The characteristic hexagonal crystal habit of ZnO is clearly visible in some of the larger particles (courtesy of Dr A. Dowd). ....	178
<b>Figure 5.49.</b> FTIR spectrum of BZA dihydrate. ....	179
<b>Figure 5.50.</b> CP-MAS $^{13}\text{C}$ NMR spectra of BZA. ....	180
<b>Figure 5.51.</b> TGA-DTA in air on BZA with heating rate of $5\text{ }^\circ\text{C min}^{-1}$ . ....	181
<b>Figure 5.52.</b> Colour-coded contour graphs generated from XRD (synchrotron) data show the real-time transformation of BZA to ZnO. The intensity is colour-coded. Top and bottom contour graphs show different ranges of $2\theta$ vs. temperature. ....	182
<b>Figure 5.53.</b> 3D-stacked XRD (synchrotron) graphs from different views and in different ranges of temperatures for clarity. ....	183
<b>Figure 5.54.</b> XRD data collected from 27 to $113\text{ }^\circ\text{C}$ in a synchrotron. $2\theta$ values are converted to corresponding $\text{Cu K}\alpha$ values for comparison reasons. Peaks marked with * correspond to ZnO and stick lines correspond to anhydrous zinc acetate (JC-PDF 00-001-0089). ....	184
<b>Figure 5.55.</b> XRD ( $\text{Cu K}\alpha$ ) on the product collected after heating at $90\text{ }^\circ\text{C}$ shows the presence of ZnO mixed with anhydrous zinc acetate and a phase reported to be $\text{Zn}_3(\text{OH})_4(\text{Ac})_2$ . ....	186
<b>Figure 5.56.</b> TGA-MS data produced by the decomposition of aged zinc hydroxy acetate under argon atmosphere at a heating rate of $3\text{ }^\circ\text{C min}^{-1}$ . Channels $I_{44}$ ( $\text{CO}_2$ ), $I_{18}$ ( $\text{H}_2\text{O}$ ), $I_{32}$ ( $\text{O}_2$ ), $I_{60}$ (acetic acid) and $I_{58}$	

(acetone) are scaled $\times 10^{10}$ , $\times 10^9$ , $\times 10^{10}$ and $\times 10^{12}$ and $\times 10^{11}$ , respectively. (Channel $I_{102}$ (acetic anhydride) data comes from a separate but similar sample of BZA to the other data (scaled $\times 10^{14}$ )).	187
<b>Figure 5.57.</b> TGA-DTA on zinc acetate dihydrate in air. (I) heating rate: $1\text{ }^{\circ}\text{C min}^{-1}$ and (II) heating rate $5\text{ }^{\circ}\text{C min}^{-1}$ .	190
<b>Figure 5.58.</b> Sublimation apparatus to trap the volatile zinc-bearing material.	191
<b>Figure 5.59.</b> XRD of the sublimate collected during thermal decomposition of dehydrated BZA.	192
<b>Figure 5.60.</b> SEM images of the sublimate.	192
<b>Figure 5.61.</b> XRD on (I) BZA and (II) the freeze-dried product of the reaction between BZA and ethanol. Peaks marked with ‘*’ correspond to ZnO (JC-PDF 01-089-0510).	194
<b>Figure 5.62.</b> TGA on (I) BZA and (II) the freeze-dried product of the reaction between BZA and ethanol.	195
<b>Figure 5.63.</b> DTA on (I) BZA and (II) the freeze-dried product of the reaction between BZA and ethanol.	195
<b>Figure 5.64.</b> Raman spectra corresponding to (I) BZA and (II) product of the reaction between BZA and ethanol, freeze-dried for 24 hours.	197
<b>Figure 5.65.</b> FT-IR spectra corresponding to (I) BZA and (II) product of the reaction between BZA and ethanol, freeze-dried for 24 hours.	198
<b>Figure 5.66.</b> CP-MAS $^{13}\text{C}$ NMR spectrum of the product of the reaction between BZA and ethanol, freeze-dried for 24 hours.	199
<b>Figure 5.67.</b> TGA in air on basic zinc salts with heating rate of $5\text{ }^{\circ}\text{C min}^{-1}$ .	200
<b>Figure 5.68.</b> XRD (synchrotron) on the precursor basic zinc salts.	201
<b>Figure 5.69.</b> XRD (synchrotron) on the end-products of the corresponding basic zinc salts at the maximum temperature during synchrotron radiation study. (Data have been normalised to beam intensity here and everywhere else in this thesis).	202
<b>Figure 5.70.</b> Fluorescence emission spectra of ZnO powder samples made from: (I) basic zinc carbonate at $300\text{ }^{\circ}\text{C}$ ; (II) basic zinc sulphate at $900\text{ }^{\circ}\text{C}$ ; (III) basic zinc acetate at $400\text{ }^{\circ}\text{C}$ ; (IV) basic zinc nitrate at $400\text{ }^{\circ}\text{C}$ ; (V) basic zinc chloride at $600\text{ }^{\circ}\text{C}$ . (VI) is emission spectrum of commercial Zn:ZnO phosphor as a control. Excitation wavelength = $280\text{ nm}$ , excitation slit width = $5\text{ nm}$ (little steps at $460$ and $570\text{ nm}$ are artefacts due to filter changes).	203
<b>Figure 5.71.</b> RT fluorescence emission spectra of ZnO powder samples made from: (I) basic zinc carbonate at $300\text{ }^{\circ}\text{C}$ ; (II) basic zinc sulphate at $900\text{ }^{\circ}\text{C}$ ; (III) basic zinc acetate at $400\text{ }^{\circ}\text{C}$ ; (IV) basic zinc nitrate at $400\text{ }^{\circ}\text{C}$ ; (V) basic zinc chloride at $600\text{ }^{\circ}\text{C}$ . (VI) is the emission spectrum of commercial Zn:ZnO phosphor as a control. Excitation wavelength = $310\text{ nm}$ , excitation slit width = $5\text{ nm}$ (little steps at $460$ and $570\text{ nm}$ are artefacts due to filter changes).	203
<b>Figure 5.72.</b> Colour-coded (top) 3D contour and (bottom) 2D top RT fluorescence emission spectra of Zn:ZnO phosphor vs. excitation wavelength from $300$ to $400\text{ nm}$ .	204
<b>Figure 6.1.</b> XRD on the products of Reactions A - D and the precipitate from the filtrate of Reaction A.	213
<b>Figure 6.2.</b> TGA of the products of Reaction A-D and the precipitate from the filtrate of Reaction A.	215



---

<b>Figure 6.3.</b> DTA of the products of Reaction A to D and the precipitate from the filtrate of Reaction A (graphs are offset for clarity).....	216
<b>Figure 6.4.</b> SEM images on the zinc hydroxy nitrate precipitated from the filtrate of Reaction A. ....	217
<b>Figure 6.5.</b> Gibbs free energy of Reaction 6.9 is positive at $t = 0$ . As time passes, it becomes negative (over $t_{eq} \approx 20$ minutes) and reaches its minimum at around 75 minutes. Then it approaches zero again at around 180 minutes due to the change in $Q_r$ (as a result of changes in concentrations of the species in solution). ....	222
<b>Figure 6.6.</b> XRD patterns of the samples collected in the course of reaction. ....	223
<b>Figure 6.7.</b> TGA on the samples collected in the course of reaction. ....	224
<b>Figure 6.8.</b> DTA on the samples collected in the course of reaction (graphs are offset for clarity). ....	224
<b>Figure 6.9.</b> Graph of $\ln(\ln(\text{conversion}))$ vs. $\ln(\text{time})$ is not linear. ....	225
<b>Figure 6.10.</b> Sigmoid function curve fitting for conversion vs. time and the 1 <sup>st</sup> and 2 <sup>nd</sup> derivatives of the fitted curve vs. time. Maximum rate of conversion was shown to be at around 75 minutes. ....	225
<b>Figure 6.11.</b> SEM images on the samples collected at times 2, 5, 10 and 15 minutes in the course of reaction.....	227
<b>Figure 6.12.</b> SEM images on the samples collected at times 20 to 240 minutes in the course of reaction. ....	228
<b>Figure 6.13.</b> Schematic of the suggested mechanism for the solid/liquid reaction between ZnO and zinc nitrate solution. $H^+$ shows a catalytic role in this system. ....	231

## List of Tables

	<b>Page</b>
<b>Table 1.1.</b> Typical properties of different grades of zinc oxide according to ASTM D4295-89 [44]. Reproduced with permission, from ASTM D4295-89 (2005) Standard Classification for Rubber Compounding Materials-Zinc Oxide, copyright ASTM International, 100 Barr Harbor Drive, West Conshohocken, PA 19428. ....	11
<b>Table 1.2.</b> Industrial grades of zinc oxide. Data are adapted from the product datasheets from industrial producers: PT. Indo Lysaght Indonesia, US Zinc in the USA, Umicore Zinc Chemicals and Silox in Belgium, IEQSA in Peru and Grillo Zinkoxid GmbH in Germany. ....	43
<b>Table 1.3.</b> Skincare products containing active ZnO vs. its percentage in the formulation [212]. ....	58
<b>Table 2.1.</b> Zinc sulphate to sodium hydroxide mole ratio. The pH of the resultant mixtures after reaction was in the range of 11 to 12. ....	81
<b>Table 5.1.</b> Calcination conditions to produce ZnO using basic zinc salt precursors. ....	125
<b>Table 5.2.</b> TGA-MS experiments conditions and species tested. ....	161
<b>Table 5.3.</b> Ion intensity fraction for NO (X), NO <sub>2</sub> (Y) and O <sub>2</sub> (Z) vs. rate of heating. ....	166
<b>Table 5.4.</b> Layered zinc hydroxy-acetates of the Zn <sub>x</sub> (OH) <sub>y</sub> Ac <sub>z</sub> ·nH <sub>2</sub> O family, Ac = acetate [CH <sub>3</sub> CO <sub>2</sub> ] <sup>-</sup> . The interlayer <i>d</i> -spacings are obtained from the text of the source or by analysing the published X-ray diffraction pattern. ....	172
<b>Table 5.5.</b> FTIR spectral assignments for BZA. ....	179
<b>Table 5.6.</b> BET specific surface area of the ZnO powder samples vs. precursor salt and calcination temperature. ....	205
<b>Table 6.1.</b> Mole ratios of the reactants and pH data. ....	211
<b>Table 6.2.</b> Reaction data from solid/liquid reactions between ZnO and Zn(NO <sub>3</sub> ) <sub>2</sub> . ....	215
<b>Table 6.3.</b> Difference between the measured and calculated equilibrium pH of zinc nitrate solution. The pH is calculated based on the hydrolysis reaction $Zn^{2+}_{(aq)} + H_2O \rightleftharpoons ZnOH^+_{(aq)} + H^+_{(aq)}$ . ....	219
<b>Table 6.4.</b> Solubility products of some zinc compounds compared to the reported values for zinc hydroxy nitrate in the current work. ....	230

---

## List of Schemes

	<b>Page</b>
<b>Scheme 2.1.</b> Thermodynamic data for the formation of ZnO from $Zn^{2+}$ and $OH^-$ at 298 °K and 1 atm. Standard states have been assumed. For consistency, data from Zhang and Muhammed were used [289]. .....	97
<b>Scheme 3.1.</b> Thermodynamic data for the formation of ZnO from $Zn^{2+}$ -water-ammonia system at 298 °K and 1 atm. Standard states have been assumed. Data adopted from [89, 285, 289].	107
<b>Scheme 5.1.</b> Schematic of suggested mechanism for thermal transformation of $BZS \cdot 4H_2O$ into ZnO. Dotted arrows show partial side reaction. ....	142
<b>Scheme 5.2.</b> Schematic of suggested mechanism for thermal transformation of $BZCl$ into ZnO. Partial side reaction is indicated by dotted arrow, which is responsible for the excess of mass loss during some TGA experiments. ....	156
<b>Scheme 5.3.</b> Schematic of suggested mechanism for thermal transformation of $BZN$ to ZnO. Dotted arrows represent probable side reactions that are not balanced. ....	169
<b>Scheme 5.4.</b> Schematic of suggested mechanism for thermal transformation of $BZA \cdot 2H_2O$ to ZnO. Dotted arrows show side reactions. ....	193

## Abbreviations

$\alpha_L$  = coefficient of expansion

$\lambda$  = thermal conductivity value

**Ac** = acetate ( $\text{CH}_3\text{CO}_2^-$ )

ASTM = American Society for Testing and Materials

a.m.u = atomic mass unit

BAW = bulk acoustic wave

BET = Brunauer, Emmett and Teller

BZA = basic zinc acetate

BZC = basic zinc carbonate

BZCl = basic zinc chloride

BZN = basic zinc nitrate

BZS = basic zinc sulphate

CHM = composite hydroxide mediated

$C_p^\circ$  = specific heat capacity

CP-MAS = cross polarisation magic angle spinning

cr = crystalline

CRT = cathode ray tube

CVD = chemical vapor deposition

D2EHPA = di-2-ethyl hexyl phosphoric acid

DMS = dilute magnetic semiconductors

DSC = dust settling chamber

DTA = Differential thermal analysis

$E_a$  = apparent activation energy

EAFD = electric arc furnace dust

EG = ethylene glycol

ENR = epoxidised natural rubber

EPDM = ethylene propylene diene monomer

FID = Free induction decay

FTIR = Fourier transform infrared

FWHM = Full width at half maximum

G = Gibbs free energy

GTL = gas-to-liquid

H = Enthalpy

H<sub>2</sub>O<sub>2</sub> = hydrogen peroxide

HCE = hexachloroethane

HDPE = high density polyethylene

HDS = hydroxy double salts

HVPE = hydride vapor phase deposition

ICP-MS = Inductively coupled plasma mass spectrometry

ISP = imperial smelting process/irregularly-shaped particle

ITO = indium tin oxide

$K_{\text{atm}}$  = equilibrium constant

LDH = layered double hydroxide

LED = light emitting diodes

MBE = molecular beam epitaxy

MBT = mercaptobenzothiazole

MCP = mechano-chemical process

MOCVD = metal organic chemical vapor deposition

MS = mass spectrometry

M.W = molecular weight

$\text{Na}_2\text{S}_2\text{O}_4$  = sodium dithionite

$\text{NaHSO}_2 \cdot \text{CH}_2\text{O} \cdot 2\text{H}_2\text{O}$  = sodium formaldehyde sulfoxylate

NMR = Nuclear magnetic resonance

OECD = Organisation for Economic Cooperation and Development

PFD = process flow diagram

phr = parts per hundred

PMA = polymer-modified asphalts

PP = polypropylene

ppb = parts per billion

ppm = parts per million

PVC = poly vinyl chloride

PVDF = polyvinylidene fluoride

rpm = revolutions per minute

RT = room temperature

SAW = surface acoustic wave

SRB = sulphate-reducing bacteria

SEM = scanning electron microscopy

SHG = special high grade

s-SBR = solution styrene-butadiene rubber

SVP = seeded vapor phase

T = temperature

TCO = transparent conductive oxides

TE = thermoelectric

TEM = transmission electron microscopy

TG = thermogravimetric

TGA = thermogravimetric analysis

TMTD = tetra-methyl-thiuramdisulphide

UV = ultra violet

VLS = vapor-liquid-solid

VPT = vapor phase transport

VS = vapor-solid

w/v = weight to volume

w/w = weight to weight

XNBR = carboxylated nitrile rubber

XRD = X-ray diffraction

ZnAc<sub>2</sub> = zinc acetate

Zn(CH<sub>3</sub>COO)<sub>2</sub>·2H<sub>2</sub>O = zinc acetate dihydrate

ZDDP = Zinc dialkyldithiophosphate

ZnSO<sub>4</sub>·7H<sub>2</sub>O = zinc sulphate heptahydrate

ZT = figures-of-merit

**Publications and conference presentations associated with this work**

1. Moezzi, A., “Nano vs. Active Zinc Oxide”. Presentation at the International Conference on Nanosciences and Nanotechnology (ICONN), Sydney, Australia, February 2010.
2. Moezzi, A., Cortie, M and McDonagh, A. “Aqueous pathways for the formation of zinc oxide nanoparticles”. Dalton Transactions **40**(18) (2011) 4871-4878.
3. Moezzi, A., Cortie, M and McDonagh, A. “Zinc Oxide Particles: Synthesis, Properties and Applications”. Chemical Engineering Journal **185-186** (2012) 1-22.



## Abstract

Zinc oxide is an important material industrially and scientifically. It has a long history dating back to more than four thousand years ago. It has applications in rubber production, cosmetics, pigments and ceramics. The properties of zinc oxide such as porosity, specific surface area and optical properties change as a result of changing the synthetic method and process conditions. The suitability of ZnO for different applications depends on the properties of the material, which in turn are influenced by synthetic routes.

Knowledge of the processes underpinning the various synthetic techniques is key to understanding the properties of the ZnO end-product. In this work, various synthetic techniques have been investigated that may be amenable to large-scale production. The resultant materials were studied and important insights were obtained. For example, it was found that the precursor materials and method of processing for the production of zinc oxide have important roles in controlling the properties of the product such as specific surface area, crystal morphology, particle size and amount of surface hydroxyl groups embedded in the product.

In single-stage production methods, zinc oxide is precipitated directly from a zinc solution. Influences of reaction temperature, concentration of the reactants and feeding techniques on the properties of the products were determined.

In multi-stage routes, intermediate zinc-bearing materials including zinc peroxide and zinc hydroxy carbonate, sulphate, chloride, nitrate and acetate were synthesised. These intermediate materials were then used as precursors for the formation of zinc oxide particles. Relationships between the properties of the precursor zinc-containing compound and the end-product zinc oxide were studied and unexpected results were obtained. For example, it was shown that specific surface area of the zinc oxide product depends significantly on the precursor material from which it is produced. Techniques were investigated that can produce multiple important zinc-bearing compounds and it was found that it could be engineered by selection of the appropriate precursors and process conditions.